

Effect of breakup processes on the near-barrier elastic scattering of the ${}^6,7\text{Li} + {}^{232}\text{Th}$ systems

Shradha Dubey,^{1,2} S. Mukherjee,¹ D. C. Biswas,^{2,*} B. K. Nayak,² D. Patel,¹ G. K. Prajapati,² Y. K. Gupta,² B. N. Joshi,² L. S. Danu,² S. Mukhopadhyay,² B. V. John,² V. V. Desai,² S. V. Suryanarayana,² R. P. Vind,² N. N. Deshmukh,¹ S. Appannababu,¹ and P. M. Prajapati¹

¹*Physics Department, Faculty of Science, M.S. University of Baroda, Vadodara 390002, India*

²*Nuclear Physics Division, Bhabha Atomic Research Centre, Mumbai 400085, India*

(Received 7 August 2013; revised manuscript received 25 November 2013; published 15 January 2014)

Elastic scattering angular distribution measurements of the weakly bound ${}^6,7\text{Li}$ projectiles on a ${}^{232}\text{Th}$ target have been carried out at different bombarding energies close to the Coulomb barrier. The data have been analyzed for both systems using the optical model ECIS code with phenomenological Woods-Saxon and Sao Paulo double-folding forms of the optical potentials. The energy dependence of the volume-type real and imaginary parts of the optical potentials are derived from the best fit of the experimental angular distribution data. The usual threshold anomaly has been observed for the ${}^7\text{Li} + {}^{232}\text{Th}$ system, whereas there is an indication of a breakup threshold anomaly in case of the ${}^6\text{Li} + {}^{232}\text{Th}$ system. Results on total reaction cross sections obtained from the optical model analysis for both systems have been interpreted to understand the role of projectile breakup on the reaction mechanism.

DOI: [10.1103/PhysRevC.89.014610](https://doi.org/10.1103/PhysRevC.89.014610)

PACS number(s): 25.70.Bc, 24.10.Ht, 25.70.Mn

I. INTRODUCTION

The study of elastic scattering around the Coulomb barrier is important to determine the energy dependence of potential parameters for the real and the imaginary parts of the nuclear interaction in order to understand the coupling of intrinsic degrees of freedom to the relative motion of the colliding nuclei. From the systematic analysis of elastic scattering measurements involving tightly bound nuclei, a phenomenon called the “threshold anomaly” (TA) has been observed in a number of systems [1–4]. A characteristic localized peak in the real part and the corresponding decrease of the imaginary part of the potential are observed as the bombarding energy decreases below the Coulomb barrier. This has been understood in terms of coupling of the elastic channel to the direct reaction channels that generate an additional attractive real dynamical polarization potential, which results in a decrease of the Coulomb barrier and enhancement of the fusion cross section.

There has been renewed interest in elastic scattering studies using weakly bound projectiles, with the observation of the rapid variation of the optical potential parameters with energies around the Coulomb barrier. The study of the TA has become one of the tools to investigate the influence of the breakup and other reaction mechanisms on the elastic and fusion channels [5]. In the case of elastic scattering for the ${}^7\text{Li}$ projectile on different targets such as ${}^{59}\text{Co}$ [6], ${}^{80}\text{Se}$ [7], ${}^{138}\text{Ba}$ [8], and ${}^{208}\text{Pb}$ [9], the conventional TA has been identified. In these measurements, an increase in the real part of the potentials at energies around the Coulomb barrier was observed, indicating the presence of the usual TA. The TA situation is not clear in the case of the ${}^6\text{Li}$ projectile, which has no bound excited state and breaks up into $\alpha + d$ at 1.48 MeV, whereas ${}^7\text{Li}$ has one bound excited state at 0.48 MeV and breaks up into $\alpha + t$

at 2.47 MeV. A different type of energy dependence from that of the TA is observed for the scattering of loosely bound projectiles; this has been known as the “breakup threshold anomaly” (BTA) [10,11]. In the case of the BTA, a repulsive polarization potential is generated due to the coupling of breakup channels to the elastic scattering, which causes an increase in the imaginary potential and corresponding decrease in the real part. Several earlier works on the elastic scattering of ${}^6\text{Li}$ on various targets such as ${}^{27}\text{Al}$ [12], ${}^{64}\text{Ni}$ [13], ${}^{64}\text{Zn}$ [14], ${}^{80}\text{Se}$ [7], ${}^{90}\text{Zr}$ [15], ${}^{116,112}\text{Sn}$ [16], ${}^{138}\text{Ba}$ [8], ${}^{144}\text{Sm}$ [17], ${}^{208}\text{Pb}$ [9], and ${}^{209}\text{Bi}$ [18] have indicated that results are compatible with the absence of the conventional TA. In these cases it has been observed that there are small increases in the imaginary part of the optical potential rather than decreasing to zero at energies below the Coulomb barrier, indicating the absence of the normal TA. Contradictory results have been reported for ${}^{138}\text{Ba}$ [10] and ${}^{28}\text{Si}$ [19] targets, where the BTA has been observed for both ${}^6,7\text{Li}$ projectiles. However, this observation must be supported by more experimental data. In particular, there is a lack of data with heavy targets, where the strong Coulomb field may induce different behavior than with lighter targets. The motivation of the present work is to investigate the TA and the BTA by elastic scattering measurements using a heavy target (${}^{232}\text{Th}$), where the Coulomb effects will be more pronounced. The present data for ${}^6,7\text{Li} + {}^{232}\text{Th}$ reactions, supported by those available in the literature [5–18], can help to understand the overall trends in the TA and the BTA for loosely bound nuclei.

In the present work, elastic scattering angular distribution measurements have been carried out for ${}^6,7\text{Li} + {}^{232}\text{Th}$ systems at energies from 25% below the Coulomb barrier ($V_{\text{lab}} = 32$ MeV) to approximately 40% above the barrier. The total reaction cross sections for these systems have also been derived to understand the role of projectile breakup on the total reaction cross sections. The present article has been organized in the following way. The experimental setup is described in Sec. II. Data analyses using both the Wood-Saxon potential (WSP)

*dcbiswas@barc.gov.in

and double-folding Sao Paulo potential (SPP) to determine the energy dependence of potential parameters is discussed in Sec. III. The dispersion relation (DR) analysis is discussed in Sec. IV. In Sec. V, a systematic study of the total reaction cross section for ${}^{6,7}\text{Li} + {}^{232}\text{Th}$ systems is discussed. In Sec. VI, a summary and conclusions of the present work are reported.

II. EXPERIMENTAL DETAILS

The experiment was performed at the 14UD BARC-TIFR Pelletron Accelerator Facility at Mumbai using beams of ${}^{6,7}\text{Li}$ in a wide energy range around the Coulomb barrier, i.e., 24, 26, 30, 32, 35, 40, and 44 MeV for the ${}^7\text{Li} + {}^{232}\text{Th}$ system and 26, 30, 32, 35, 40, and 44 MeV for the ${}^6\text{Li} + {}^{232}\text{Th}$ system. The observed uncertainty in the beam energy was about 1% for all the selected energies. A self-supporting 1.6 mg/cm^2 thick ${}^{232}\text{Th}$ target was placed at the center of the general purpose scattering chamber and the elastically scattered ${}^{6,7}\text{Li}$ particles were detected by ΔE - E telescopes mounted on a movable arm of the chamber. Four telescopes of thicknesses T_1 with $\Delta E = 25\text{ }\mu\text{m}$ and $E = 300\text{ }\mu\text{m}$, T_2 with $\Delta E = 15\text{ }\mu\text{m}$ and $E = 1500\text{ }\mu\text{m}$, T_3 with $\Delta E = 15\text{ }\mu\text{m}$ and $E = 1000\text{ }\mu\text{m}$, and T_4 with $\Delta E = 15\text{ }\mu\text{m}$ and $E = 1000\text{ }\mu\text{m}$ were used in the experiment. The detector telescopes were placed at an angular separation of 10° and two $300\text{-}\mu\text{m}$ -thick monitor detectors were mounted at fixed angles of $\pm 15^\circ$ with respect to the beam direction for absolute normalization and beam monitoring. The angular distributions were measured in steps of 5° in the angular range from 20° to 170° . The uncertainty on the angular range of each telescope was $\pm 0.68^\circ$. A typical bi-parametric ΔE - E_{res} spectrum for the ${}^7\text{Li} + {}^{232}\text{Th}$ system at $E_{\text{lab}} = 44\text{ MeV}$ and $\theta_{\text{lab}} = 60^\circ$ is plotted in Fig. 1, showing the isotopic separation of the reaction products. In the inset of Fig. 1, the projection onto the E_{res} axis for the $Z = 3$ events has been plotted. For angular distribution studies, the area of

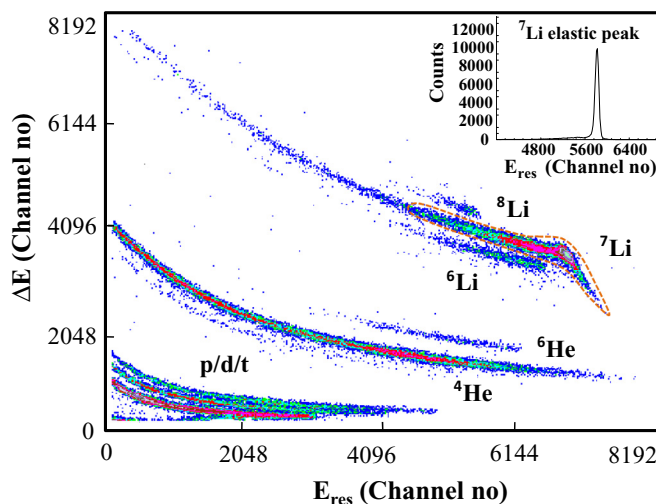


FIG. 1. (Color online) A typical two-dimensional ΔE vs E_{res} spectrum for the ${}^7\text{Li} + {}^{232}\text{Th}$ system at $E_{\text{lab}} = 44\text{ MeV}$ and $\theta_{\text{lab}} = 60^\circ$. The projection of the ${}^7\text{Li}$ elastic peak of the bi-parametric ΔE vs E_{res} spectrum is shown in the inset.

the elastically scattered peak was obtained at various angles for all energies.

III. OPTICAL MODEL ANALYSIS OF ELASTIC SCATTERING

In this section the procedure for analyzing the elastic scattering angular distribution data is presented. Two different types of optical model potential have been used in order to check whether the results show any dependence on the theoretical models. In Sec. III A the analysis with a phenomenological Woods-Saxon form interaction potential is described, and in Sec. III B the analysis performed by using the double-folding SPP is presented [20,21].

A. Analysis with phenomenological Woods-Saxon potential

The optical model fits to the elastic scattering data have been performed using the ECIS code [22]. The phenomenological Woods-Saxon form of the interaction potential with only volume terms has been used in the analysis. To obtain the starting parameters, a global best-fit procedure for all energies was performed, using the three parameters characterized by the real and imaginary depth of the potential, reduced radii (r_o), and the diffuseness (a_v and a_w). Thereafter, in order to avoid a fit procedure with too many parameters, the real and imaginary reduced radii were fixed at 1.06 fm for both ${}^{6,7}\text{Li} + {}^{232}\text{Th}$ systems, which is similar to the value used earlier [16]. This analysis procedure has been successfully adopted in the past by several groups [8,12,13,16,17,19,23]. By using this radius, and varying the diffuseness parameters a_v and a_w (real and imaginary, respectively) within the interval from 0.67 fm to 0.75 fm , an attempt was made to obtain the best possible parameters for the optical potential to describe the elastic scattering angular distribution. In the present work, the best possible fitted values were obtained for $a_v, a_w = 0.71\text{ fm}$. The real and imaginary radius parameters ($r_o = 1.06\text{ fm}$) and diffuseness parameters ($a_v, a_w = 0.71\text{ fm}$) were fixed for all energies. The depths of the real and imaginary potentials were varied to obtain the minimum value of χ^2 for both ${}^{6,7}\text{Li} + {}^{232}\text{Th}$ systems. The potential parameter values for the best fit and the total reaction cross section are listed in Table I and Table II for

TABLE I. Optical model parameters obtained by fitting the experimental elastic differential cross section data using the ECIS code (with $a_o = 0.71\text{ fm}$ and $r_o = 1.06\text{ fm}$) and SPP calculations for the ${}^7\text{Li} + {}^{232}\text{Th}$ system.

| E_{lab} (MeV) | Wood Saxon potential | | | | Sao Paulo potential | | | |
|---------------------------|----------------------|-------------|--------------------|-----------------|---------------------|-------|--------------------|-----------------|
| | V_r (MeV) | V_i (MeV) | $\frac{\chi^2}{n}$ | σ_R (mb) | N_R | N_I | $\frac{\chi^2}{n}$ | σ_R (mb) |
| 24 | 70.200 | 13.70 | 1.66 | 0.129 | 0.81 | 0.36 | 1.66 | 0.114 |
| 26 | 85.000 | 19.70 | 1.66 | 0.919 | 0.94 | 0.45 | 1.57 | 0.807 |
| 30 | 95.220 | 30.70 | 2.72 | 20.07 | 1.55 | 0.55 | 2.01 | 18.90 |
| 32 | 360.00 | 58.54 | 0.38 | 260.8 | 2.00 | 0.56 | 0.36 | 260.6 |
| 35 | 157.90 | 73.62 | 1.11 | 470.7 | 0.88 | 0.61 | 1.19 | 471.9 |
| 40 | 147.42 | 78.34 | 2.73 | 967.7 | 0.83 | 0.60 | 2.82 | 959.7 |
| 44 | 115.80 | 67.66 | 2.66 | 1215 | 0.66 | 0.53 | 2.89 | 1213 |

TABLE II. Optical model parameters obtained by fitting the experimental elastic differential cross section data using the ECIS code (with $a_o = 0.71$ fm and $r_o = 1.06$ fm) and SPP calculations for the ${}^6\text{Li} + {}^{232}\text{Th}$ system.

| E_{lab} (MeV) | Wood Saxon potential | | | | Sao Paulo potential | | | |
|---------------------------|----------------------|-------------|--------------------|-----------------|---------------------|-------|--------------------|-----------------|
| | V_r (MeV) | V_i (MeV) | $\frac{\chi^2}{n}$ | σ_R (mb) | N_R | N_I | $\frac{\chi^2}{n}$ | σ_R (mb) |
| 26 | 105.6 | 90.00 | 2.33 | 3.884 | 0.72 | 1.06 | 1.92 | 3.57 |
| 30 | 263.3 | 167.7 | 1.70 | 105.4 | 1.41 | 1.72 | 2.08 | 107.0 |
| 32 | 215.9 | 394.6 | 2.37 | 404.4 | 1.29 | 3.68 | 2.64 | 398.4 |
| 35 | 130.2 | 183.5 | 1.02 | 561.2 | 0.82 | 1.52 | 1.45 | 550.6 |
| 40 | 97.69 | 136.0 | 2.39 | 970.6 | 0.87 | 1.09 | 2.71 | 963.6 |
| 44 | 128.8 | 144.7 | 0.68 | 1336 | 0.80 | 1.24 | 0.51 | 1335 |

${}^7\text{Li} + {}^{232}\text{Th}$ and ${}^6\text{Li} + {}^{232}\text{Th}$ systems, respectively. The best-fit optical model parameters show significant energy dependence as reflected from Table I and Table II, which is a characteristic feature of elastic scattering. Figures 2 and 3 show the best fit of the experimental data for the elastic scattering angular distributions for ${}^7\text{Li} + {}^{232}\text{Th}$ and ${}^6\text{Li} + {}^{232}\text{Th}$ systems.

Very good fits to the data were obtained, and expectedly it was found that several families of optical potential describe the angular distributions equally well. To reduce the ambiguities of the best-fitted parameters for the optical potential, the strong sensitive radii R_{Sr} and R_{Si} corresponding to the real and imaginary potential were determined. For this purpose the radius parameters were kept fixed and the depth parameters of the real and imaginary potentials were fitted by varying the diffuseness from 0.67 to 0.75 fm, in steps of 0.02 fm for all the energies of ${}^6,7\text{Li} + {}^{232}\text{Th}$ systems. The strong sensitive radii [24] were determined by where the real and the imaginary

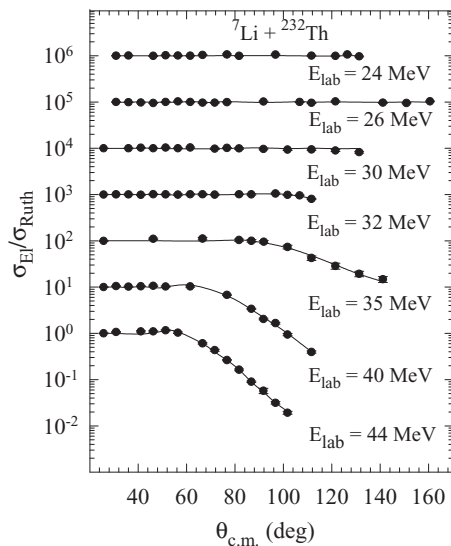


FIG. 2. Experimental elastic scattering cross section (σ_{EI}) normalized to the Rutherford cross section (σ_{Ruth}) as a function of $\theta_{\text{c.m.}}$ for the ${}^7\text{Li} + {}^{232}\text{Th}$ system (solid circles) (suitably scaled up for each energy) and their best fits from optical model calculations (solid lines). The curves correspond to the best fits obtained by using the ECIS code.

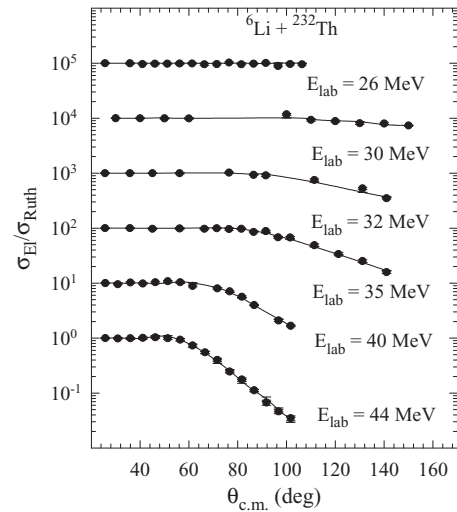


FIG. 3. Experimental elastic scattering cross section (σ_{EI}) normalized to the Rutherford cross section (σ_{Ruth}) as a function of $\theta_{\text{c.m.}}$ for the ${}^6\text{Li} + {}^{232}\text{Th}$ system (solid circles) (suitably scaled up for each energy) and their best fits from optical model calculations (solid lines). The curves correspond to the best fits obtained by using the ECIS code.

parts of different optical potentials that fitted the data cross each other, as shown in Fig. 4(a) and 4(b) at 44 MeV for the ${}^6\text{Li} + {}^{232}\text{Th}$ system. For the ${}^7\text{Li} + {}^{232}\text{Th}$ system the real sensitive radii values are observed to be in the range of 12.6 to 9.5 fm with an average of $R_{Sr} = 11.5$ fm and the imaginary sensitive radii values range from 12.7 to 8.5 fm with an average value of $R_{Si} = 11.05$ fm. A mean sensitive radius of $R_s = 11.27$ fm for the ${}^7\text{Li} + {}^{232}\text{Th}$ system (the average between $R_{Sr} = 11.50$ fm and $R_{Si} = 11.05$ fm) was obtained to derive the energy dependence of the real and imaginary potentials. Similarly for the ${}^6\text{Li} + {}^{232}\text{Th}$ system, the average sensitive radius was $R_s = 12.14$ fm (the average between $R_{Sr} = 12.05$ fm, and $R_{Si} = 12.23$ fm). The values of radius parameters for the real and imaginary parts were kept fixed at 1.06 fm for all the calculations for ${}^6,7\text{Li} + {}^{232}\text{Th}$ systems in the analysis. A similar fitting procedure can also be found in the literature [8,15,16].

B. Analysis using the double-folding Sao Paulo potential

The SPP [20,21] is an optical potential that has been successfully used to describe a large variety of systems in a wide energy range, including fusion excitation functions and barrier distributions of weakly bound nuclei [25,26]. This potential is based on the Pauli nonlocality involving the exchange of nucleons between the projectile and the target. For a limited range of energy, as in the present work, it can be considered as the usual double-folding potential based on an extensive systematization of nuclear densities extracted from elastic scattering data. The imaginary part of the interaction is assumed to have the same shape as the real part, with one single adjustable parameter N_I related to its strength. The data-fit procedure is performed with only two free parameters, the normalization factors for the real and the imaginary parts,

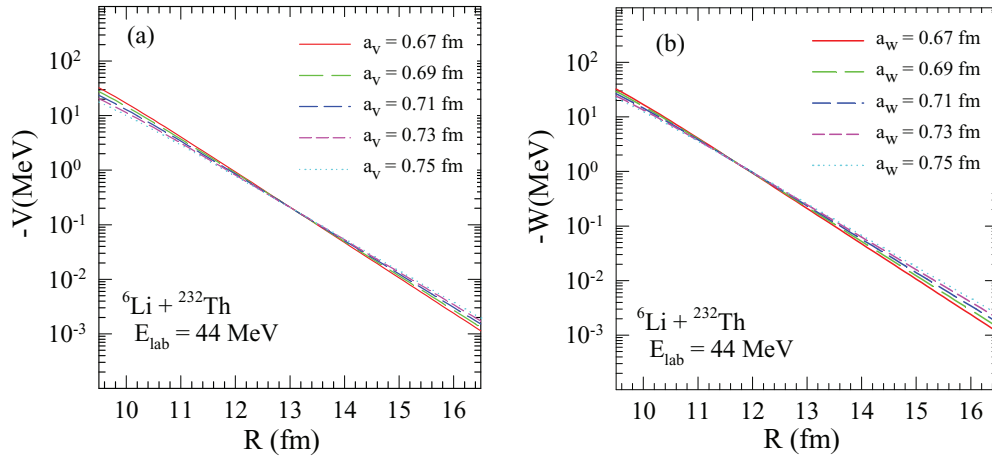


FIG. 4. (Color online) Several potentials that produce similar fits of the data, for 44 MeV. The crossing point are the derived real (a) and imaginary (b) sensitivity radii.

N_R and N_I . The energy-dependent normalization coefficients N_R and N_I take into account the effects of the dynamical polarization potential due to direct channel couplings. These dynamical polarization potentials are directly related to a dispersion relation. The present elastic scattering angular distribution analysis with the Sao Paulo potential follows the prescription given by Gomes *et al.* [10]. The curves resulting from the best fits using the SPP overlap with the calculations of the Wood-Saxon potential and therefore are not shown in Figs. 2 and 3. The resulting fits of the normalization parameters are listed in Tables I and II for ${}^7\text{Li} + {}^{232}\text{Th}$ and ${}^6\text{Li} + {}^{232}\text{Th}$ systems, respectively. It can be observed that the energy dependence (Fig. 6) follows the results from previous analysis similarly. So, our conclusions concerning the behavior of the optical potential energy dependence do not change when either of the potentials is used.

IV. DISPERSION RELATION ANALYSIS

An elastic scattering dispersion relation analysis has been carried out for ${}^6,7\text{Li} + {}^{232}\text{Th}$ systems in order to qualitatively understand the experimental results on the energy dependence of the real and imaginary potentials. In the study of the dispersion relation, the optical potentials are fixed and only the depth parameters are varied so that it is valid at all radii. The dispersion relation for the optical model of elastic scattering is given as [1,2,27,28]

$$\Delta V(E) = \frac{P}{\pi} \int_{-\infty}^{+\infty} \frac{W(E')}{E' - E} dE', \quad (1)$$

where P denotes the principal value. Equation (1) allows us to evaluate ΔV , the dispersive contribution to the real part, from knowledge of empirical values of the optical model absorption term $W(E)$ at sensitive radius.

Equation (1) indicates that, at energies where the absorption increases rapidly, the real part of the potential gets more attractive (i.e., ΔV is negative) than in the regions where the absorption remains constant or changes gradually [29]. This behavior has indeed been observed at energies near the top of the Coulomb barrier, where the rapid variation in the

strength of the empirical real part has been called the threshold anomaly. According to the dispersion relation formulation, this variation in $V(E)$ is related to the rapid changes occurring in the imaginary term due to the opening of reaction channels as the Coulomb barrier is surpassed. In this work, the dispersion relation has been applied as a function of E at the sensitive radius (R_s) to the phenomenological optical model potentials, determined at each energy between 24 to 44 MeV for both ${}^6,7\text{Li} + {}^{232}\text{Th}$ systems. The linear segment model proposed in Ref. [30] was used in the imaginary part in order to get the real part. In the ${}^7\text{Li} + {}^{232}\text{Th}$ system, three sets of the real potential $V(E)$ were obtained by numerical integration of Eq. (1) using three sets of different line segment fits of the imaginary potential $W(E)$ [29]. Similarly, the energy dependence of the real and the imaginary parts of the SPP are shown in Fig. 6. N_R is obtained by means of the dispersion relation using the same procedure as in the case of the phenomenological potential previously described. One can observe results similar to those from the WSP approach. In the past, several studies were carried out in order to observe the energy-dependent behavior of the real and imaginary parts of the optical potential in the dispersion relation calculations near and below the barrier energies [8,10–12,15–18]. However, in some recent studies [8,10], important differences in the interpretation of the dispersion relations of the two lithium isotopes around the barrier energies have arisen. Figure 5 shows the energy dependence of the potential parameters for both systems ${}^6,7\text{Li} + {}^{232}\text{Th}$. The solid points represent the values of the real and the imaginary potentials derived by using the sensitivity radius using the Wood Saxon optical potential. The solid and the dashed curves represent the analysis using the dispersion relation. Similarly, Fig. 6 shows the energy dependence of the normalization factors N_R and N_I , for the real and the imaginary potentials with the SPP (solid points). The solid and dashed curves indicate the behavior of N_R and N_I with the dispersion relation. In the case of the ${}^7\text{Li} + {}^{232}\text{Th}$ system, both analyses show similar trends (Figs. 5 and 6). It can be clearly seen that the real potential first increases and then decreases below the barrier, while the imaginary part of the potential decreases below the barrier. This behavior is

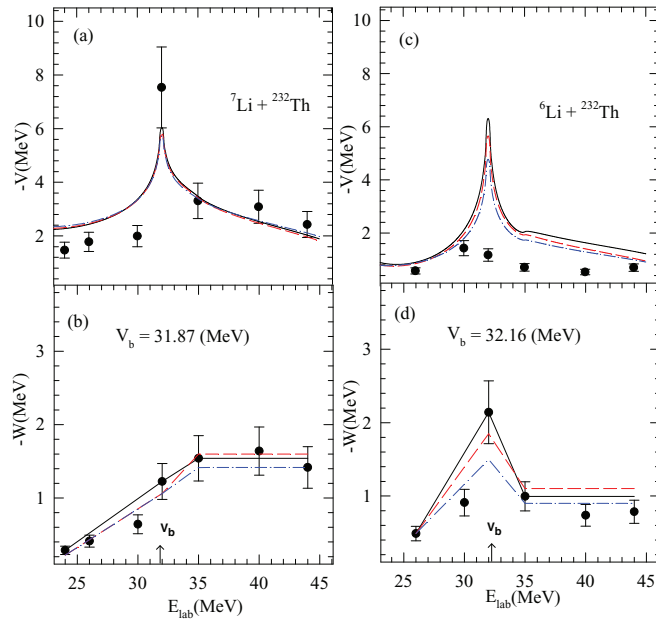


FIG. 5. (Color online) Energy dependence of the real and imaginary potentials at $R_s = 12.14$ fm and 11.27 fm for ${}^6\text{Li} + {}^{232}\text{Th}$ and ${}^7\text{Li} + {}^{232}\text{Th}$ systems, respectively. The straight line segments represent various fits of imaginary potential $W(E)$; the corresponding curves for real potential $V(E)$ were obtained from these by using the dispersion relation. Panels (a) and (b) correspond to the real and imaginary potential curves for the ${}^7\text{Li} + {}^{232}\text{Th}$ system, whereas (c) and (d) represent the ${}^6\text{Li} + {}^{232}\text{Th}$ system.

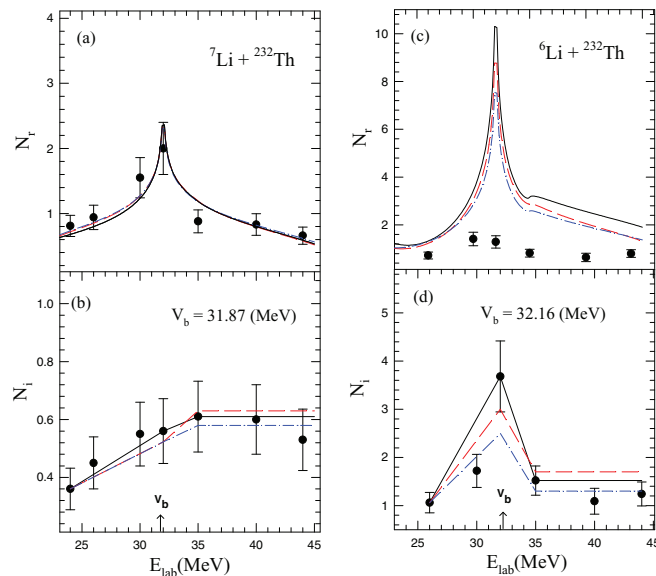


FIG. 6. (Color online) Energy dependence of the normalization factors N_R and N_I , for the real and imaginary potentials, corresponding to the Sao Paulo potential with two free parameters, for the ${}^6\text{Li} + {}^{232}\text{Th}$ and ${}^7\text{Li} + {}^{232}\text{Th}$ systems. The lines represent possible behaviors of N_R and N_I that are compatible with the dispersion relation [2,10]. Panels (a) and (b) correspond to the real and imaginary potential curves for the ${}^7\text{Li} + {}^{232}\text{Th}$ system, whereas (c) and (d) represent the ${}^6\text{Li} + {}^{232}\text{Th}$ system.

supported by the analysis of the dispersion relation that fits the data appreciably well. Thus it may be concluded that elastic scattering of the ${}^7\text{Li} + {}^{232}\text{Th}$ system has the usual threshold anomaly, as indicated by a characteristic localized peak in the real part and a corresponding decrease of the imaginary part of the potential as the bombarding energy decreases toward the Coulomb barrier. The present inferences are in agreement with that reported by others in the literature [8,16,31].

For the ${}^6\text{Li} + {}^{232}\text{Th}$ system, the imaginary part of the potential shows an increase, although limited to one point only, and then it decreases as the bombarding energy decreases toward the Coulomb barrier. On the other hand, the real part of the optical potential slightly increases and then shows a decreasing trend below the barrier energy. This trend is definitely in contrast to what has been observed in the case of the ${}^7\text{Li} + {}^{232}\text{Th}$ system. This is an indication of the absence of a normal TA in the ${}^6\text{Li} + {}^{232}\text{Th}$ system. This is obvious because, in the reactions with the ${}^6\text{Li}$ projectile, breakup is

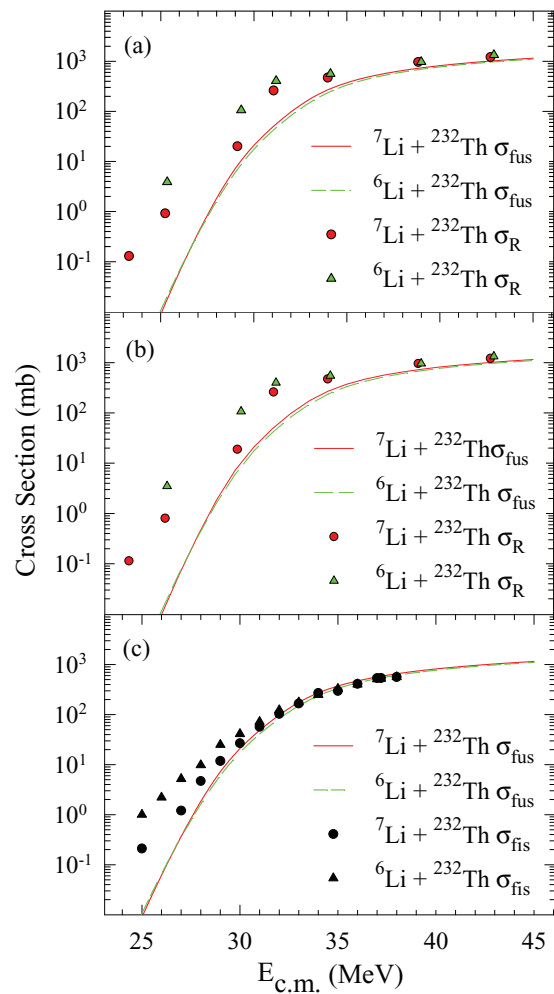


FIG. 7. (Color online) The total fusion cross sections (σ_{fus}) calculated by CCFULL and total reaction cross sections (σ_R) for the ${}^6,{}^7\text{Li} + {}^{232}\text{Th}$ systems obtained by using (a) the ECIS code and (b) the SPP calculation, plotted as a function of the bombarding energy. The total fission cross sections (σ_{fis}) [33] and the total fusion cross sections for the ${}^6,{}^7\text{Li} + {}^{232}\text{Th}$ systems are plotted in (c).

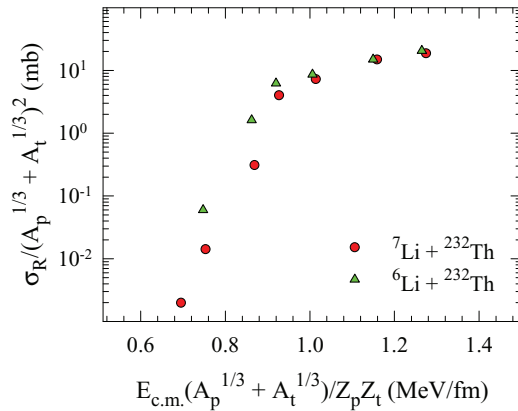


FIG. 8. (Color online) Reduced total reaction cross section vs reduced projectile energy for the $^{6,7}\text{Li} + ^{232}\text{Th}$ reactions using the prescription given in Ref. [40].

the dominant channel, unlike in the case of the ^7Li projectile where the breakup channel is far above its first excited state. Similar results for the TA and the BTA have also been reported for $^{6,7}\text{Li} + ^{80}\text{Se}$ systems [7]. This indicates that the $^6\text{Li} + ^{232}\text{Th}$ system shows the presence of a BTA, whereas the $^7\text{Li} + ^{232}\text{Th}$ system shows a normal TA.

V. TOTAL REACTION CROSS SECTION

The fusion cross sections have been calculated for $^{6,7}\text{Li} + ^{232}\text{Th}$ systems by using the CCFULL code [32]. The energy range used in the calculation was 24 to 44 MeV, in steps of 1 MeV. In the present work, the total reaction cross sections derived from the experimental elastic scattering data for $^{6,7}\text{Li} + ^{232}\text{Th}$ systems were compared with the calculated fusion cross sections and measured fission cross section values taken from the literature [33] as shown in Figs. 7(a), 7(b), and 7(c). The total reaction cross sections obtained from the optical model ECIS code and the SPP calculation have larger values for the $^6\text{Li} + ^{232}\text{Th}$ system in comparison to the $^7\text{Li} + ^{232}\text{Th}$ system, for all energies as shown in Fig. 7. The reaction cross sections are predominantly enhanced compared to CCFULL calculations at sub-barrier energies. From Fig. 7, it is also seen that the fission cross section has a strong enhancement for the ^6Li projectile at sub-barrier energies. At above-barrier energies the fusion-fission process is dominant, but at lower energies the breakup fusion-fission process becomes important and hence the fission cross section for the $^6\text{Li} + ^{232}\text{Th}$ system is enhanced at sub-barrier energies. This may be an indication that the inclusive breakup reaction cross section is significantly more for ^6Li compared to the ^7Li projectile. These results are similar to the earlier measurements of ^6Li on

^{28}Si and ^{208}Pb [34,35], where the yield of α particles indicates the breakup contribution in ^6Li . However, more coincidence measurements with the reaction products will provide a better understanding of the enhanced breakup probability for ^6Li . The role of projectile structure in the reaction dynamics and the influence of the breakup process in the fusion cross sections at energies near the Coulomb barrier have also been reported earlier for weakly as well as tightly bound projectiles [36–39]. In order to eliminate the projectile size effects on the reaction cross sections for $^{6,7}\text{Li} + ^{232}\text{Th}$ systems, the “reduction” method was used. This method was proposed by Gomes *et al.* [40] and has been well implemented by others [16,41,42]. The reduced cross section values were calculated at all energies for both systems. In this method, the quantities $\sigma_R / (A_p^{1/3} + A_t^{1/3})^2$ versus $E_{c.m.} (A_p^{1/3} + A_t^{1/3}) / Z_p Z_t$ are plotted, where P and T represent the projectile and the target, respectively, and σ_R is the total reaction cross section. As shown in Fig. 8, it can be seen that the total reduced reaction cross section for ^6Li is larger than that for ^7Li , below the barrier. This is again an indication of higher breakup probability in the case of ^6Li and is also in agreement with the earlier observations [7,16,29].

VI. SUMMARY AND CONCLUSIONS

Elastic scattering angular distribution measurements have been carried out for the $^{6,7}\text{Li} + ^{232}\text{Th}$ systems at several bombarding energies from below to well above the Coulomb barrier. The experimental data have been analyzed by using the WSP and SPP double-folding forms of phenomenological optical potentials. The relevant parameters that give a best fit to the elastic scattering angular distribution were obtained through a χ^2 -minimization procedure. The behavior of the corresponding parts of the potential as a function of energy is consistent with a situation close to the threshold anomaly for the $^7\text{Li} + ^{232}\text{Th}$ system. The increasing trend around the barrier of the imaginary part of the phenomenological potential as a function of energy indicates the absence of the usual threshold anomaly for the $^6\text{Li} + ^{232}\text{Th}$ system and this may be interpreted as evidence of the breakup threshold anomaly. The enhanced reaction cross sections have been observed at sub-barrier energies for the $^6\text{Li} + ^{232}\text{Th}$ system in comparison to the $^7\text{Li} + ^{232}\text{Th}$ system. It will be interesting to have more exclusive measurements in order to understand the higher breakup probabilities for the ^6Li projectile.

ACKNOWLEDGMENTS

We thank the operating staff of the BARC-TIFR Pelletron, Mumbai, India, for the smooth running of the machine during the experiment. SD and SM acknowledge UGC-DAE-CSR, Kolkata, for financial support through a major research project.

- [1] M. A. Nagarajan, C. C. Mahaux, and G. R. Satchler, *Phys. Rev. Lett.* **54**, 1136 (1985).
- [2] G. R. Satchler, *Phys. Rep.* **199**, 147 (1991).
- [3] M. E. Brandan and G. R. Satchler, *Phys. Rep.* **285**, 143 (1997).
- [4] P. Singh, S. Kailas, A. Chatterjee, S. S. Kerekatte, A. Navin, A. Nijasure, and B. John, *Nucl. Phys. A* **555**, 606 (1993).
- [5] J. Lubian *et al.*, *Nucl. Phys. A* **791**, 24 (2007).

- [6] F. A. Souza *et al.*, *Phys. Rev. C* **75**, 044601 (2007).
- [7] L. Fimiani *et al.*, *Phys. Rev. C* **86**, 044607 (2012).
- [8] A. M. M. Maciel *et al.*, *Phys. Rev. C* **59**, 2103 (1999).
- [9] N. Keeley, S. J. Bennett, N. M. Clarke, B. R. Fulton, G. Tungate, P. V. Drumm, M. A. Nagarajan, and J. S. Lilley, *Nucl. Phys. A* **571**, 326 (1994).
- [10] P. R. S. Gomes *et al.*, *J. Phys. G* **31**, S1669 (2005).

- [11] M. S. Hussein, P. R. S. Gomes, J. Lubian, and L. C. Chamon, *Phys. Rev. C* **73**, 044610 (2006).
- [12] J. M. Figueira *et al.*, *Phys. Rev. C* **75**, 017602 (2007).
- [13] M. Biswas *et al.*, *Nucl. Phys. A* **802**, 67 (2008).
- [14] M. Zadro *et al.*, *Phys. Rev. C* **80**, 064610 (2009).
- [15] H. Kumawat *et al.*, *Phys. Rev. C* **78**, 044617 (2008).
- [16] N. N. Deshmukh *et al.*, *Phys. Rev. C* **83**, 024607 (2011).
- [17] J. M. Figueira *et al.*, *Phys. Rev. C* **81**, 024613 (2010).
- [18] S. Santra, S. Kailas, K. Ramachandran, V. V. Parkar, V. Jha, B. J. Roy, and P. Shukla, *Phys. Rev. C* **83**, 034616 (2011).
- [19] A. Gomez Camacho, P. R. S. Gomes, and J. Lubian, *Phys. Rev. C* **82**, 067601 (2010).
- [20] L. C. Chamon, D. Pereira, M. S. Hussein, M. A. Candido Ribeiro, and D. Galetti, *Phys. Rev. Lett.* **79**, 5218 (1997).
- [21] L. C. Chamon *et al.*, *Phys. Rev. C* **66**, 014610 (2002).
- [22] J. Raynal, *Phys. Rev. C* **23**, 2571 (1981).
- [23] D. Patel *et al.*, *Pramana-J. Phys.* **81**, 587 (2013).
- [24] G. R. Satchler, in *Proceedings of the International Conference on Reactions between Complex Nuclei, Nashville, TN*, edited by R. L. Robinson, F. K. McGowan, J. B. Ball, and J. H. Hamilton (North Holland, Amsterdam, 1974), Vol. 2, p. 171.
- [25] E. Crema, L. C. Chamon, and P. R. S. Gomes, *Phys. Rev. C* **72**, 034610 (2005).
- [26] E. Crema, P. R. S. Gomes, and L. C. Chamon, *Phys. Rev. C* **75**, 037601 (2007).
- [27] B. R. Fulton, D. W. Banes, J. S. Lilley, M. A. Nagarajan, and I. J. Thompson, *Phys. Lett. B.* **162**, 55 (1985).
- [28] A. Baeza, B. Bilwes, R. Bilwes, J. Diaz, and J. L. Ferrero, *Nucl. Phys. A* **419**, 412 (1984).
- [29] M. M. Gonzalez and M. E. Brandan, *Nucl. Phys. A* **693**, 603 (2001).
- [30] C. Mahaux, H. Ngo, and G. R. Satchler, *Nucl. Phys. A* **449**, 354 (1986).
- [31] N. Keeley and K. Rusek, *Phys. Rev. C* **56**, 3421 (1997).
- [32] K. Hagino *et al.*, *Comput. Phys.* **123**, 143 (1999).
- [33] H. Freiesleben, G. T. Rizzo, and J. R. Huizenga, *Phys. Rev. C* **12**, 42 (1975).
- [34] A. Pakou *et al.*, *Phys. Rev. Lett. B* **633**, 691 (2006).
- [35] C. Signorini *et al.*, *Phys. Rev. C* **67**, 044607 (2003).
- [36] M. Dasgupta *et al.*, *Nucl. Phys. A* **834**, 147c (2010).
- [37] M. Dasgupta *et al.*, *Phys. Rev. Lett.* **82**, 1395 (1999).
- [38] D. C. Biswas, R. K. Choudhury, D. M. Nadkarni, and V. S. Ramamurthy, *Phys. Rev. C* **52**, 2827 (1995).
- [39] D. C. Biswas, R. K. Choudhury, B. K. Nayak, D. M. Nadkarni, and V. S. Ramamurthy, *Phys. Rev. C* **56**, 1926 (1997).
- [40] P. R. S. Gomes, J. Lubian, I. Padron, and R. M. Anjos, *Phys. Rev. C* **71**, 017601 (2005).
- [41] N. N. Deshmukh *et al.*, *Eur. Phys. J. A* **47**, 118 (2011).
- [42] S. Mukherjee *et al.*, *Eur. Phys. J. A* **45**, 23 (2010).